frontiers in
PHARMACOLOGY

ORIGINAL RESEARCH ARTICLE
published: 28 March 2012
doi: 10.3389/fphar.2012.00053

Restraint stress intensifies interstitial K^+ accumulation during severe hypoxia

Christian Schnell[1,2†‡], Oliwia A. Janc[1,2‡], Belinda Kempkes[2], Carolina Araya Callis[1,3], Gabriele Flügge[1,3], Swen Hülsmann[1,2†] and Michael Müller[1,2]*

[1] DFG Research Center Molecular Physiology of the Brain, Georg-August-Universität Göttingen, Göttingen, Germany
[2] Abteilung Neuro- und Sinnesphysiologie, Zentrum für Physiologie und Pathophysiologie, Georg-August-Universität Göttingen, Göttingen, Germany
[3] Klinische Neurobiologie, Deutsches Primatenzentrum Göttingen, Göttingen, Germany

Edited by:
Amalia M. Dolga, Philipps-Universität Marburg, Germany

Reviewed by:
Palle Christophersen, NeuroSearch A7S, Denmark
Yi Dong, Fudan University, China

***Correspondence:**
Michael Müller, Zentrum Physiologie und Pathophysiologie, Universität Göttingen, Humboldtallee 23, D-37073 Göttingen, Germany.
e-mail: mmuelle7@gwdg.de

†Present Address:
Christian Schnell and Swen Hülsmann, Abteilung Neurophysiologie und Zelluläre Biophysik, Zentrum Physiologie und Pathophysiologie, Georg-August-Universität Göttingen, Göttingen, Germany.

‡Christian Schnell and Oliwia A. Janc have contributed equally to this work.

Chronic stress affects neuronal networks by inducing dendritic retraction, modifying neuronal excitability and plasticity, and modulating glial cells. To elucidate the functional consequences of chronic stress for the hippocampal network, we submitted adult rats to daily restraint stress for 3 weeks (6 h/day). In acute hippocampal tissue slices of stressed rats, basal synaptic function and short-term plasticity at Schaffer collateral/CA1 neuron synapses were unchanged while long-term potentiation was markedly impaired. The spatiotemporal propagation pattern of hypoxia-induced spreading depression episodes was indistinguishable among control and stress slices. However, the duration of the extracellular direct current potential shift was shortened after stress. Moreover, K^+ fluxes early during hypoxia were more intense, and the postsynaptic recoveries of interstitial K^+ levels and synaptic function were slower. Morphometric analysis of immunohistochemically stained sections suggested hippocampal shrinkage in stressed rats, and the number of cells that are immunoreactive for glial fibrillary acidic protein was increased in the CA1 subfield indicating activation of astrocytes. Western blots showed a marked downregulation of the inwardly rectifying K^+ channel Kir4.1 in stressed rats. Yet, resting membrane potentials, input resistance, and K^+-induced inward currents in CA1 astrocytes were indistinguishable from controls. These data indicate an intensified interstitial K^+ accumulation during hypoxia in the hippocampus of chronically stressed rats which seems to arise from a reduced interstitial volume fraction rather than impaired glial K^+ buffering. One may speculate that chronic stress aggravates hypoxia-induced pathophysiological processes in the hippocampal network and that this has implications for the ischemic brain.

Keywords: spreading depression, anoxia, hippocampus, spatial buffering, synaptic function

INTRODUCTION

Repeated stressful experiences have a profound impact on neuronal plasticity in the hippocampal formation (for review see Fuchs et al., 2006; Popoli et al., 2012). Among the underlying cellular changes, dendritic remodeling of hippocampal pyramidal neurons has been documented after chronic stress exposure (Magariños et al., 1996, 1997; Kole et al., 2004), and the regression of the geometrical length of apical dendrites of CA3 pyramidal neurons is probably the most thoroughly investigated anatomical change (Watanabe et al., 1992). Such alterations in dendritic morphology directly affect neuronal functioning as a shortening of even a few dendrites has been shown to enhance backpropagation of action potentials (Golding et al., 2001; Schaefer et al., 2003). Furthermore, the stress-induced decrease in the apical dendritic length of CA3 pyramidal neurons in rat hippocampus correlated with a reduced membrane time constant and input resistance as well as an increased subthreshold excitability (Kole et al., 2004).

Dendritic architecture is also closely correlated with the degree of connectivity within neuronal networks. In hippocampal pyramidal neurons, extensive dendritic sprouting, and enhanced spine density were observed when the number of axonal afferents was increased (Kossel et al., 1997), whereas the loss of afferents induced dendritic atrophy (Valverde, 1968; Benes et al., 1977; Deitch and Rubel, 1984).

Also glutamatergic synaptic transmission has been found to be affected markedly by stress. Various models of acute or chronic stress as well as glucocorticoid treatment were reported to modify glutamate release and uptake, but also to exert an effect on glutamate metabolism, as well as the expression and possibly the subunit composition of the various glutamate receptors (for review see Popoli et al., 2012). Especially these changes in the function of glutamatergic synapses are considered crucial for the remarkable impact of chronic stress on neuronal plasticity, the reduction of long-term potentiation (LTP), and the associated impairment of various cognitive processes (Pavlides et al., 2002).

In addition to neurons, also glial cells are affected by stress. Chronic immobilization stress in rats increased glial fibrillary acidic protein (GFAP) expression which indicates reactive gliosis (Jang et al., 2008), whereas chronic social stress in male tree shrews reduced both the number and soma volume of hippocampal astrocytes (Czéh et al., 2006).

This variety of morphological and molecular changes induced by stress in neurons and glial cells reflects a remarkable remodeling of neuronal networks which may include alterations in their functioning and plasticity already under physiological conditions. Hence, neuronal networks of chronically stressed subjects can be expected to be more vulnerable to additional pathophysiological events.

The hippocampus and especially the pyramidal neurons of the CA1 subfield are among those parts of the brain being most vulnerable to metabolic compromise such as anoxia/ischemia (Pulsinelli et al., 1982; Schmidt-Kastner and Freund, 1991). Within just a few minutes of oxygen (O_2) shortage, neuronal function is massively impaired bearing the risk of sustained and irreversible damage. We therefore analyzed the impact of chronic restraint stress on the responses of the hippocampal network to severe hypoxia.

Adult rats were exposed to an established chronic restraint stress protocol and the outcome of such treatment on hippocampal network function was analyzed under normoxic and hypoxic conditions. Emphasis of our analyses was on the early network responses to severe hypoxia (O_2 withdrawal), i.e., the concerted massive depolarizations of cellular elements that give rise to the phenomenon of hypoxia-induced spreading depression (HSD). This integrated network response is associated with a (temporary) loss of neuronal excitability and synaptic transmission, and it represents an experimental model of, e.g., cerebral stroke (for review see Gorji, 2001; Somjen, 2001; Lauritzen et al., 2011). Electrophysiological analyses in acute hippocampal tissue slices, complemented by optical imaging and immunolabeling, revealed an intensified interstitial K^+ accumulation during early hypoxia as well as a delayed posthypoxic recovery, and a more severe impairment of synaptic function in chronically stressed rats as compared to controls.

MATERIALS AND METHODS

RESTRAINT STRESS

Adult male Sprague Dawley rats (Harlan-Winkelmann) weighing between 250 and 300 g on arrival were housed in groups ($n = 3$) in type II macrolon cages with food and water *ad libitum* under an inverse light–dark cycle (lights off 7:00 AM–7:00 PM) at 21 ± 1°C. All animal experiments were performed in accordance with the directive of November 24, 1986 of The Council of the European Communities (86/609/ECC), including Position 6106/20 of May 26, 2010, and were approved by the Lower Saxony Federal State Office for Consumer Protection and Food Safety, Germany.

After 2 weeks of habituation, animals were chronically exposed to restraint stress according to an established paradigm (Magariños and McEwen, 1995; Magariños et al., 1997). Chronic stress consisted of immobilizing rats daily during their activity period for 6 h, during 3 weeks. For restraint, animals were placed in well ventilated plastic tubes in their home cages; during this time they had no access to food and water (**Figure 1A**). On the day after the last stress exposure brains were dissected and taken into the experiments. Control rats were handled daily at the same time and had no access to food and water during the daily restraint session, but experienced no restraint stress.

Chronic restraint stress is known to reduce body weight gain (Watanabe et al., 1992). Therefore, to confirm that the stress procedure was effective, rats were weighed on the last day of this treatment. As expected, body weight in the stressed rats was significantly reduced by an average of 17.2% (control 375.8 ± 49.6 g, $n = 35$; stress 311.2 ± 27.2 g, $n = 34$). Moreover, the stress increased the relative adrenal weight (adrenal weight in mg/100 g body weight) by 25.4% indicating hyperactivity of the hypothalamic–pituitary adrenal axis, which represents a characteristic stress response (control 0.138 ± 0.018 g; stress 0.173 ± 0.013 g, $n = 14$ each).

PREPARATION

Acute hippocampal tissue slices were prepared from ether anesthetized rats. Following decapitation the brain was rapidly removed from the skull and placed in chilled artificial cerebrospinal fluid (ACSF) for 1–2 min. The two hemispheres were separated, and 400 μm slices were cut using a vibroslicer (Campden Instruments, 752M Vibroslice or Leica VT1000S). Slices were then transferred either to a storage chamber (kept at room temperature) or an interface recording chamber of the Oslo style and left undisturbed for at least 90 min. The interface chamber was kept at 35–36°C, aerated with 95% O_2–5% CO_2 (400 ml/min), and perfused with oxygenated ACSF (3–4 ml/min).

SOLUTIONS

Chemicals were obtained from Sigma-Aldrich unless otherwise mentioned. ACSF had the following composition (in mM): 130 NaCl, 3.5 KCl, 1.25 NaH_2PO_4, 24 $NaHCO_3$, 1.2 $CaCl_2$, 1.2 $MgSO_4$, and 10 dextrose; aerated with 95% O_2–5% CO_2 to adjust pH to 7.4.

MICROELECTRODES

Single barreled glass microelectrodes for extracellular recordings were pulled from thin-walled borosilicate glass (GC150TF-10, Harvard Apparatus) using a horizontal puller (P-97, Sutter Instruments). They were filled with ACSF and their tips were broken to a final resistance of 5–10 MΩ. Patch-pipettes were made from borosilicate glass capillaries (Biomedical Instruments) on a horizontal pipette-puller (Zeitz-Instrumente) and filled with (in mM) 125 κ-Gluconate, 1 $CaCl_2$, 2 $MgCl_2$, 4 Na_2-ATP, 10 EGTA, 10 HEPES (pH adjusted to 7.2 with KOH). Electrode resistance ranged from 4 to 7 MΩ.

Changes in the extracellular K^+ concentration $[K^+]_o$ were continuously monitored using double-barreled K^+ selective microelectrodes of the twisted type. Two borosilicate glass capillaries – one with and one without filament (GC150-15 and GC100F-15, Harvard Apparatus) – were glued together with epoxy glue (for details see Hepp and Müller, 2008; Fischer et al., 2009). Electrodes were pulled on a vertical electrode puller (Narishige PE-2). First, capillaries were pulled by 3–4 mm, while twisting the reference barrel around the center capillary. In a second step capillaries were then pulled apart. The ion-selective barrel was silanized by HMDS vapors (hexamethyldisilazane, 98%, Fluka; 40°C, 45 min exposure), for protection from HMDS the reference barrel was filled with distilled water. Subsequently electrodes were incubated in the oven (200°C, 2 h).

The tip of the K^+-sensitive barrel was filled with the valinomycin based K^+ ion neutral carrier (Potassium Ionophore I – Cocktail A, Fluka 60031) and backfilled with 150 mM

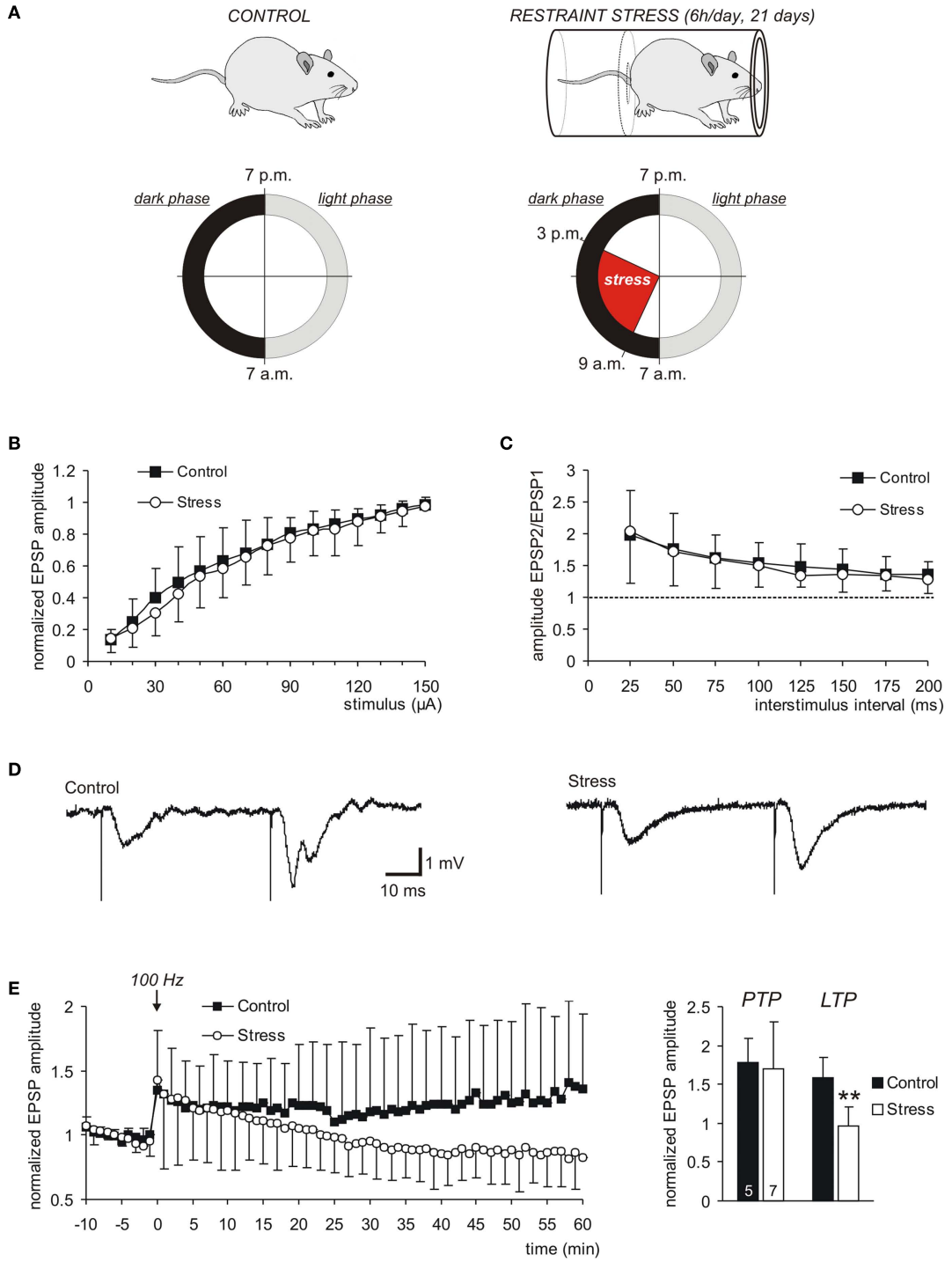

FIGURE 1 | Chronic restraint stress leaves basal synaptic function intact but impairs LTP. (A) Control and stressed rats were kept under an inverse light–dark cycle. For a total duration of 21 days they were exposed to restraint stress during their activity periods. **(B)** As indicated by the input–output curves, basal synaptic transmission at the Schaffer collateral/CA1 pyramidal neuron synapse was not affected by chronic stress. The averages of 16 control and 15 stress slices are plotted, error bars represent standard deviations. **(C)** PPF, recorded in the same set of slices, was not affected by chronic stress. **(D)** Sample traces of fEPSPs recorded in control and stress slices. **(E)** In stress slices, stable LTP could not be induced. The LTP-inducing stimulus was delivered at time 0 (arrow mark) and evoked an indistinguishable PTP in both groups. In stress slices, however, the amplitude of the fEPSPs then declined to pre-stimulus baseline conditions in the course of the next 60 min ($n = 5$ control, $n = 7$ stress slices). For clarity, error bars were omitted for every second data point. The bar plot summarizes the averaged fEPSP amplitudes right after the 100 Hz stimulus (PTP) as well as in the time window of 50–60 min later (LTP). The number of slices analyzed is indicated at the bottom of the bars; asterisks indicate statistically significant changes ($^{**}P < 0.01$).

KCl + 10 mM HEPES, pH 7.4. The reference barrel was filled with 150 mM NaCl + 10 mM HEPES, pH 7.4 (Müller and Somjen, 2000a). Tip resistances of the ion-selective and reference barrel were 170–250 and 10–20 MΩ, respectively. Electrodes were calibrated before/after each experiment using standard solutions of 0, 1, 2, 5, 10, 20, 50, and 100 mM K^+. Constant ionic strength of these solutions was maintained by replacing Na^+ by K^+ and *vice versa*. Average slope and detection limit of the K^+ selective electrodes were 54.9 ± 3.5 mV/decade K^+ and 0.72 ± 0.53 mM K^+ ($n = 31$), respectively. Ion-sensitive electrode signals were monitored by a differential electrometer amplifier (FD 223, World Precision Instruments) and digitized at sampling rates of 100 Hz by a Digitizer 1322A acquisition system controlled by PClamp 9.0 software (Molecular Devices), that was also used for most other electrophysiological recordings.

HYPOXIA-PROTOCOL AND ELECTRICAL RECORDINGS

Severe hypoxia was induced by switching the interface chamber's gas supply from carbogen (95% O_2–5% CO_2) to 95% N_2–5% CO_2; during that time carbogen aeration of ACSF was continued. Upon O_2 withdrawal, HSD was triggered within 2–3 min, and to ensure complete reversibility, O_2 was readmitted 25 s after HSD onset [defined as the occurrence of the sudden direct current (DC) potential deflection]. All signal amplitudes were measured between the pre-hypoxia baseline and the maximal change. Only rapid DC potential changes of at least −10 mV amplitude were considered as HSD.

Field excitatory postsynaptic potentials (fEPSPs) were elicited by 0.1 ms unipolar stimuli (Grass S88 stimulator with PSIU6 photoelectric stimulus isolation units, Grass Instruments) delivered via microwire electrodes made from bare stainless steel wire (50 µm diameter, AM-Systems) and recorded as described in detail earlier (Müller and Somjen, 1998; Hepp et al., 2005). Orthodromic responses were elicited by stimulation of Schaffer collaterals and recorded in *stratum* (*st.) radiatum* of the CA1 region, using a locally constructed extracellular DC potential amplifier. Data were sampled at 20 kHz.

For whole-cell recordings, slices were transferred to a custom-built submersion-style recording chamber mounted to an upright microscope (Axio Examiner.Z1, Zeiss) and superfused with ACSF at room temperature. Astrocytes in *st. radiatum* were identified by labeling with sulforhodamine 101 (SR101), a red fluorophore serving as a selective marker for astrocytes in hippocampus and neocortex (Nimmerjahn et al., 2004). The labeling protocol was adapted from a previous report (Kafitz et al., 2008). Briefly, slices were stained with SR101 (1 µM in ACSF, 34°C, 20 min); after washout with ACSF (10 min, 34°C), they were kept at room temperature until the recording. SR101 was excited by epifluorescence illumination (HBO100 mercury lamp; Dualband GFP/mCherry ET Filterset F56-019; AHF Analysentechnik). Since under constant excitation SR101 bleaches quickly, astrocytes – once identified – were patched using transmitted light and differential Dodt contrast (Dodt and Zieglgänsberger, 1994). Astroglial character of the cells was confirmed by their current–voltage (IV)-curves. For documentation fluorescence images of the recorded astrocytes were taken using a CCD camera (PCO; SensiCam) controlled by ImageJ software (Rasband, W.S., ImageJ, U.S. National Institutes of Health, Bethesda, MD, USA, http://imagej.nih.gov/ij/, 1997–2011).

Whole-cell voltage-clamp recordings were obtained with a Multiclamp 700A amplifier (Molecular Devices). Membrane currents were low-pass filtered at 2 kHz and digitized at 10 kHz. Voltage step protocols were performed with a Digidata 1440A interface and pClamp10 software (Molecular Devices), continuous recordings were done with a Powerlab/4S interface and Chart software (ADInstruments). Astrocytes were voltage clamped to −80 mV and the IV-curve was measured every 30 s using voltage steps to holding potentials ranging from −160 to +50 mV (10 mV increments). For the measurement of membrane resistance (R_i) astrocytes were hyperpolarized for 200 ms to −90 mV. To measure the K^+ uptake current an ACSF containing 50 mM K^+ (Na^+ replaced by K^+) was applied.

OPTICAL RECORDINGS

The characteristic intrinsic optical signal (IOS; increase in light scattering) associated with HSD was monitored with a computer-controlled imaging system (Polychrome II, Till Photonics) and a CCD camera (Imago QE, PCO Imaging) mounted to a Zeiss Axiotech microscope (Gerich et al., 2006). Slices were illuminated by white light at an angle of ∼45°; images were taken every 2 s (15 ms exposure time) using a 5×, 0.13NA objective (Epiplan, Zeiss). Changes in light reflectance of the tissue became obvious by offline image subtraction, were referred to an image taken before O_2 withdrawal (Müller and Somjen, 1999), and are displayed in a 256 gray-scale mode covering intensity changes of ±20%. Their intensity and temporal profile was analyzed within a rectangular region of interest in CA1 *st. radiatum* near the recording electrode. The propagation velocity of HSD was calculated from the progression of the reflectance increase in CA1 *st. radiatum* (parallel to *st. pyramidale*). The tissue area invaded by HSD was determined at the height of the reflectance increase. Those pixels were counted whose brightness had increased by ≥5% and were referred to the total hippocampal area. Images were processed with TILLvision4.0 (TILL Photonics) and MetaMorph6.1 (Universal Imaging Corporation).

IMMUNOHISTOCHEMISTRY

For fixation of the brains, rats were deeply anesthetized and transcardially perfused with 4% paraformaldehyde as described before (Czéh et al., 2010). Coronal 40 µm brain sections were generated with a cryostat (Leica CM3050S; −1.80 to −6.04 mm from Bregma; Paxinos and Watson, 1986).

Ten floating sections per brain were immunostained with either anti-GFAP or Kir4.1 antibody. Sections were processed in parallel to avoid variations in staining intensity. They were first washed in phosphate buffered saline (PBS) and then incubated for 30 min in 1% H_2O_2 in PBS to inactivate endogenous peroxidase activity. All following washing steps consisted of three washes of 10 min each in PBS. After washing, sections were incubated in 5% normal horse serum (Vector Laboratories), in PBS containing 0.5% Triton X-100, for 1 h to block non-specific antibody binding. For GFAP staining, sections were incubated overnight at 4°C with a mouse monoclonal anti-GFAP antibody (Sigma, clone G-A-5, No. G3893; 1:5,000 dilution) in PBS. Following washing, sections

were incubated with the secondary antibody, biotinylated horse anti-mouse IgG (Biozol, BA-2001; 1:400 dilution) in PBS for 2 h. To stain the K^+ channel subunit Kir4.1, rabbit polyclonal antibody anti-Kir4.1 (Alomone labs, product No. APC-035) was used at 1:2,000 dilution. Biotinylated goat anti-rabbit (Biozol, product No. BA-1000, 1:400 dilution) served as secondary antibody (incubation in PBS for 2 h). After washing, sections were incubated in the ABC complex (ABC Kit, Vector Laboratories) in PBS for 1.5 h. Finally, sections were incubated in 0.025% 3,3′-diaminobenzidine (DAB, Peroxidase Substrate Kit, Vector Laboratories) with 0.01% H_2O_2, washed again, mounted on glass slides, and left to dry overnight at 37°C. The following day, they were cleared in xylene and cover slipped using Eukitt mounting medium (Kindler GmbH).

To determine changes in the size of the hippocampal formation and the number of GFAP-positive cells in control and stressed rats, images of the tissue sections were acquired using a digital microscope (Nikon Coolscope; analysis software NIS-Elements AR 2.1). Cell counts and the size of the hippocampal formation were determined with the cell-counter plugin of ImageJ and MetaMorph 6.1, respectively.

WESTERN BLOT ANALYSIS

Eight rats per group were used for protein analysis. Immediately after decapitation, crania were placed on ice and the brains were quickly isolated. Hippocampi were dissected, transferred into liquid nitrogen and stored at −80°C. Hippocampi were homogenized with a dounce homogenizer (tight pestle) in ice-cold homogenization buffer (150 mM NaCl, 1 mM Tris/HCl, pH 8.0, 7% glycerol, and 0.1% Triton X-100) containing protease inhibitors (Complete Protease Inhibitor Cocktail Tablets, Roche Diagnostics). The protein homogenates were centrifuged (5 min, 13,000 rpm), supernatants recovered, and aliquots stored at −80°C. Protein concentrations were determined by Bio-Rad DC Protein assay (Bio-Rad Laboratories).

For electrophoresis, hippocampal protein extracts were denatured for 10 min at 70°C in Laemmli buffer with dithiothreitol (DTT) and chilled on ice for 5 min. After electrophoresis on a 12.5% sodium dodecyl sulfate (SDS) gel (under reducing conditions), proteins were transferred to a nitrocellulose membrane (Schleicher & Schuell) via semidry electroblotting, for 2 h at 1 mA/cm^2 in transfer buffer containing 25 mM Tris–HCl, pH 8.3, 150 mM glycine, and 10% methanol. The membrane was blocked for 1 h with 5% milk powder in PBS, and then incubated with the anti-Kir4.1 antibody (dilution 1:400) over night at 4°C. The membrane was then washed with PBS-T (0.1% Tween-20 in PBS), and incubated with goat anti-rabbit antibody, horseradish peroxidase (HRP) conjugated, dilution 1:7,500 (DakoCytomation, product No. P 0448). After 1 h of incubation at room temperature, membranes were washed three times with PBS-T and three times with PBS.

Bands were visualized by enhanced chemiluminescence (ECL; SuperSignal West Pico Kit, product No. 34079, Thermo Scientific) using Amersham Hyperfilm™ECL (GE Health Care Life Sciences). Then, in order to use β-actin as internal loading control, nitrocellulose membranes were stripped in PBS with 2% SDS, 0.7% β-mercaptoethanol, for 2 h and incubated with a monoclonal anti-β-actin antibody (Sigma, clone AC-15, product No. A 1978; 1:4,000 dilution; 30 min incubation), followed by goat anti-mouse IgG, HRP coupled (Santa Cruz Biotechnology Inc., product No. sc-2302) dilution 1:4,000, 1 h incubation. The relative optical density of the bands was quantified using ImageJ software. Intensity of the Kir4.1 band was normalized to the β-actin band, and data were presented as a percentage of the mean value from the control group.

STATISTICS

Data were obtained from 69 rats, and since most electrophysiological/IOS recordings did not last longer than ∼1.5 h, up to four slices could be used from each brain. To ensure independence of observations, each experimental treatment was performed on at least three different control and/or stressed rats. All numerical values are represented as mean ± standard deviation. Significance of the observed changes was tested using a two-tailed, unpaired Student's t-test and a significance level of 5% (unpaired observations). In the case of paired observations (i.e., the effects of repeated hypoxia in a single slice), a one-sample t-test was used to compare normalized data against pretreatment control conditions, defined as unity or as 100%. In the diagrams, significant changes are marked by asterisks ($^*P < 0.05$; $^{**}P < 0.01$; $^{***}P < 0.001$). Data processing and statistical calculations were done with Excel (Microsoft) or Sigma Stat 3.5 (Systat Software).

RESULTS

To define the outcome of chronic stress on the network function of the hippocampal circuitry, we analyzed synaptic function and plasticity as well as the responses to severe hypoxia in detailed electrophysiological, optical, and molecular biological assays.

SYNAPTIC FUNCTION AND PLASTICITY

Synaptic function and plasticity were assessed by recording evoked field potentials (fEPSPs) in *st. radiatum* of the CA1 subfield of acute hippocampal tissue slices. As indicated by the input–output curves there were no significant changes in neuronal excitability and basal synaptic function at Schaffer collateral/CA1 neuron synapses (**Figure 1B**). Also the paired-pulse facilitation (PPF), a measure for synaptic short-term plasticity, revealed no differences among control and stress slices (**Figures 1C,D**; control $n = 16$, stress $n = 15$ slices).

It has been shown before that different stress treatments or durations may suppress LTP in distinct hippocampal subfields (Pavlides et al., 2002; Buwalda et al., 2005). In the present study, induction of LTP by a single high-frequency stimulus (100 Hz, 1 s train, stimulation intensity adjusted to elicit half-maximum responses) caused a clear post-tetanic potentiation (PTP) of fEPSP amplitudes that was indistinguishable among control ($n = 5$) and stress slices ($n = 7$; **Figure 1E**). Control slices showed stable LTP with fEPSP amplitudes still being potentiated to 157.8 ± 27.0% of control, in the time window of 50–60 min after the high-frequency stimulation. In contrast, in stress slices stable LTP could not be induced. The PTP slowly decayed and fEPSP amplitudes recovered to pre-stimulus control conditions within the following 60 min (**Figure 1E**), showing that chronic restraint stress suppresses induction of LTP in the CA1 subfield.

RESPONSES TO SEVERE HYPOXIA

Previous reports have shown that exposing hippocampal slices to severe hypoxia triggers within a few minutes characteristic HSD episodes. HSD represents a propagating massive depolarization of neurons and glia that is synchronized in neighboring cells and is detectable as a sudden negative shift of the extracellular DC potential (Leão, 1947; Müller and Somjen, 2000a; Somjen, 2001).

We here show that in control slices, the DC potential shift occurred within 1.8 ± 0.4 min of O_2 withdrawal, reached an amplitude of -16.9 ± 2.3 mV, and measured at the half-maximum amplitude it lasted 52.8 ± 13.3 s ($n = 15$, **Figures 2A** and **3A**). See **Figure 2B** for a definition of these characteristic parameters of the DC potential shift. In stress slices, HSD showed a similar time to onset and DC potential amplitude, but its duration was significantly shortened to 36.6 ± 11.7 s ($n = 17$, **Figure 3A**), i.e., by an average of 30.7% as compared to controls.

In addition to the DC potential shift we also monitored changes in the interstitial K^+ concentration ($[K^+]_o$) during hypoxia, using K^+ selective microelectrodes. As defined in detail earlier (Somjen, 1979; Hansen, 1985; Müller and Somjen, 2000a), the characteristic extracellular K^+ changes during hypoxia and HSD show a typical profile consisting of (1) a linear increase early during hypoxia, before HSD onset, (2) a rapid, massive rise to a well pronounced peak as soon as HSD is triggered, and (3) a recovery upon reoxygenation which transiently undershoots the prehypoxic baseline

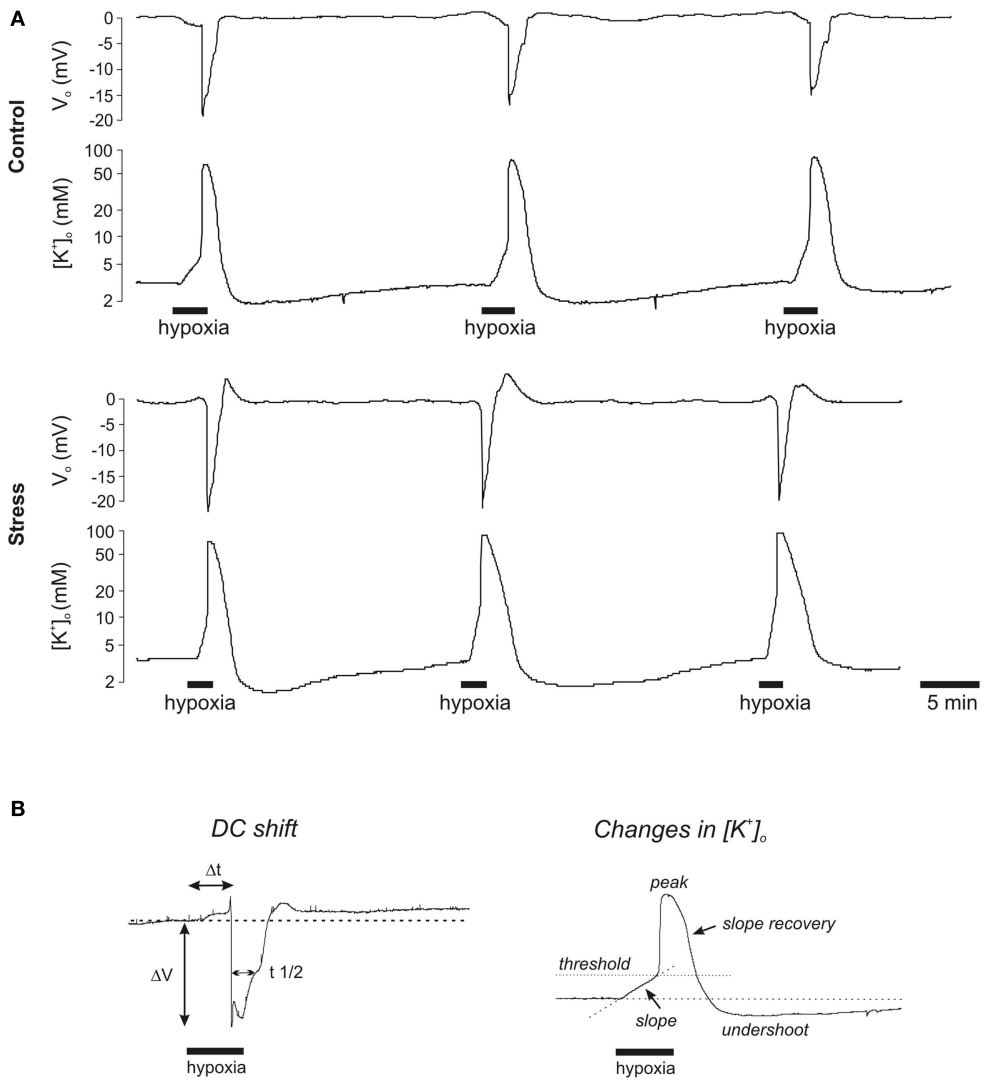

FIGURE 2 | Hypoxia-induced spreading depression episodes are not markedly affected in stressed rats. (A) Recordings of the HSD-associated negative deflection of the extracellular DC potential and the closely correlated changes in $[K^+]_o$ as monitored in *st. radiatum* of the CA1 subfield. Each slice underwent three successive hypoxic episodes. O_2 was resubmitted 25 s after the onset of the rapid DC potential deflection. Hypoxic episodes were separated by at least 20 min to ensure complete recovery. Note that stress slices showed a more rapid and intense increase in $[K^+]_o$ during early hypoxia before HSD onset and a slower posthypoxic recovery of $[K^+]_o$. **(B)** Definition of the analyzed characteristic parameters of the DC potential deflection and the associated changes in $[K^+]_o$ (ΔV amplitude of the DC shift, Δt time to onset since O_2 withdrawal, $t_{1/2}$ duration measured at the half amplitude level).

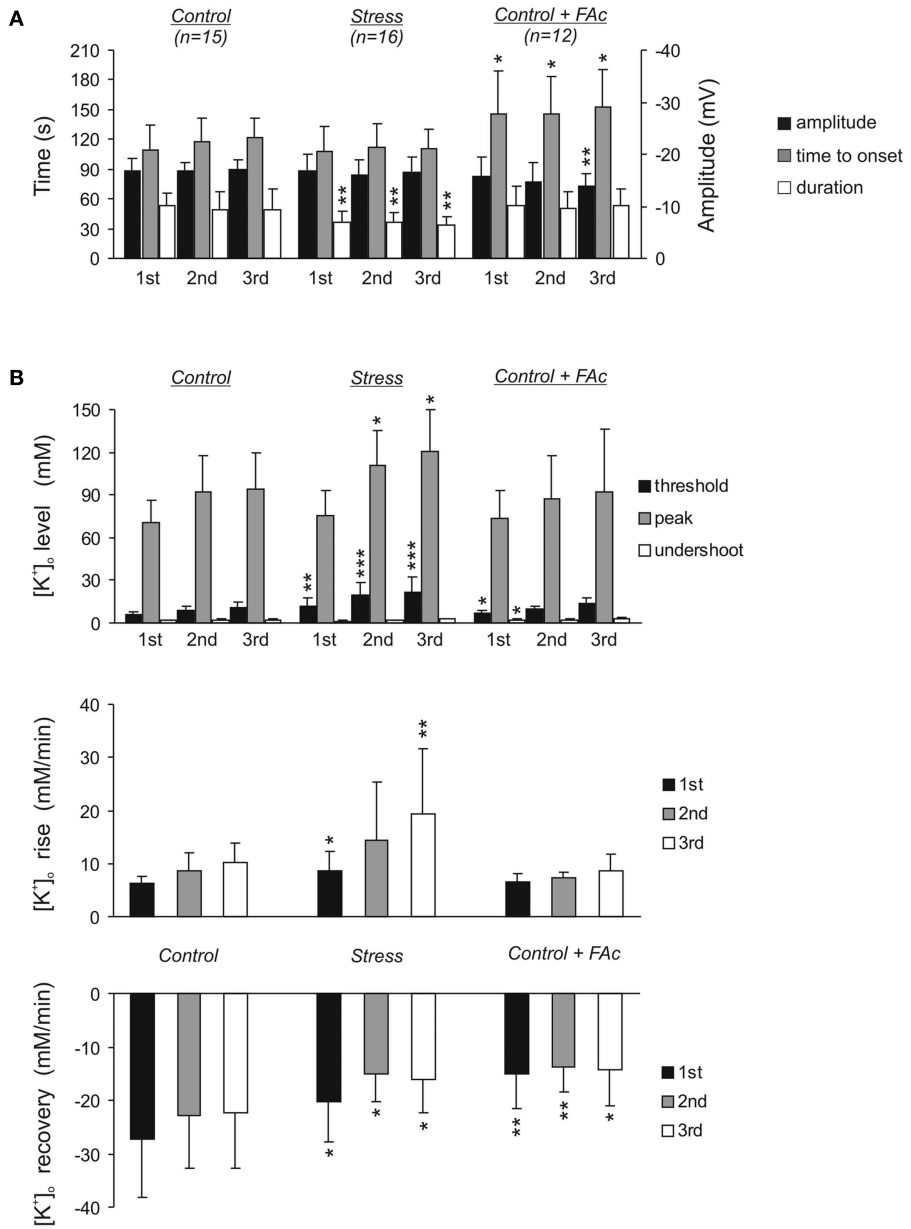

FIGURE 3 | Statistical summary of the electrophysiological signs of HSD during three consecutive episodes of hypoxia. (A) Summary of the characteristic DC potential parameters in control slices, stress slices and control slices treated with FAc (5 mM, >1.5 h). The DC potential parameters time to onset and duration refer to the left hand time axis, the amplitude refers to the right hand voltage axis. **(B)** Summary of $[K^+]_o$ at the distinct time points defined in **Figure 2B**. The lower two diagrams show the slopes of the rise in $[K^+]_o$ early during hypoxia before HSD onset and of the posthypoxic recovery, respectively. Asterisks indicate significantly different changes as compared to the respective HSD episode in control slices ($*P < 0.05$, $**P < 0.01$, $***P < 0.001$).

level. These three distinct phases could also be identified clearly in our present experiments (**Figure 2**).

In control slices, $[K^+]_o$ started to increase at a rate of 6.2 ± 1.4 mM/min as soon as O_2 was withdrawn. By the time HSD was ignited, $[K^+]_o$ had reached a threshold level of 6.2 ± 1.4 mM, and then rapidly rose further to its peak of 70.5 ± 15.9 mM. Upon reoxygenation, $[K^+]_o$ recovered at a rate of 27.4 ± 10.7 mM/min and transiently undershot the prehypoxic baseline, reaching a nadir of 1.7 ± 0.5 mM ($n = 15$, **Figures 2A** and **3B**). In stress slices, the changes in $[K^+]_o$ showed a similar profile, yet, the magnitude of the changes significantly differed from controls. During the initial phase of hypoxia before HSD onset, $[K^+]_o$ rose faster in stress slices (8.7 ± 3.7 mM/min, $n = 16$) and reached a higher threshold level of 11.6 ± 6.0 mM K^+ by the time HSD was ignited. Furthermore, the posthypoxic recovery of $[K^+]_o$ was significantly slowed down in stress slices (20.2 ± 7.5 mM/min). The peak level during

HSD and the K^+ undershoot upon reoxygenation tended to be somewhat more intense, but those differences did not reach the level of significance (**Figures 2A** and **3B**).

Since these recordings suggested a more intense response of slices from stressed rats to O_2 shortage, we also analyzed the effects of repeated hypoxia by inducing three HSD episodes in every slice (separated by recovery periods of 20 min). Again, in stress slices the duration of the second and third HSD was shorter than in controls. The slope of the initial K^+ rise and the threshold level before HSD onset became even more pronounced, the K^+ peak level during HSD was significantly higher than in control slices, and the slope of the posthypoxic recovery remained less steep (**Figure 3**).

The more intense K^+ rises early during hypoxia and during HSD as well as the slower posthypoxic recovery in stress slices may indicate impaired glial K^+ buffering. We therefore tested whether a pretreatment of slices from control rats with the glial poison fluoroacetate (FAc) would mimic the stress-mediated effects. FAc is taken up rather selectively by glial cells and, once metabolized into fluorocitrate, blocks the citric acid cycle (Clarke et al., 1970; Hassel et al., 1992). In hippocampal slices, FAc treatment is known to exert glia-specific effects such as gradual glial depolarization while pronounced neuronal damage does not occur before 8 h of treatment (Largo et al., 1996, 1997).

Fluoroacetate treatment of control slices (5 mM, >1.5 h) failed, however, to mimic the alterations induced by chronic stress. No significant changes in the characteristic HSD parameters occurred during the first two HSD episodes. The third HSD in FAc treated slices showed a reduced DC potential amplitude and occurred slightly later as compared to control slices, possibly indicating a reduced neuronal excitability and hence the onset of a FAc effect on neuronal viability (**Figure 3A**). Pronounced alterations in the HSD-related changes in $[K^+]_o$ were not observed in FAc treated slices either. Only the first HSD showed a moderate but significant increase in the threshold level before HSD onset, and the undershoot of the prehypoxic K^+ baseline during recovery was less intense. The posthypoxic recovery of $[K^+]_o$ was, however, slowed down consistently (**Figure 3B**).

SPATIOTEMPORAL PROFILE OF HSD

The IOS was monitored to define the spatiotemporal profile of HSD, i.e., its propagation within the hippocampal formation (**Figure 4A**). The IOS is a multiphasic signal consisting of a moderate initial decrease in tissue reflectance early during hypoxia, before HSD onset, which is followed by a marked increase in tissue reflectance as HSD occurs (Aitken et al., 1999; Andrew et al., 1999; Müller and Somjen, 1999; Fayuk et al., 2002). Upon reoxygenation, tissue reflectance recovers and often, a second moderate increase in tissue reflectance is observed (see e.g., arrow marks in **Figure 4B**). In the present study, our emphasis was, however, on the clear reflectance increase that coincides with the occurrence of HSD, as it unequivocally identifies those tissue areas being invaded by an HSD episode (**Figure 4A**).

In control slices, tissue reflectance increased by $11.2 \pm 5.0\%$ ($n = 16$) as HSD was ignited (analyzed in CA1 *st. radiatum*). The intensity and time course of the reflectance increase was very similar in stress slices, even when HSD was induced repeatedly. Only for the third HSD episode, somewhat less intense reflectance changes were observed in stress slices (**Figures 4B,C**). In addition, clear differences occurred during the posthypoxic recovery. In controls, a moderate secondary increase in tissue reflectance was observed which was almost absent in stress slices (**Figures 4B,D**). The propagation velocity of HSD averaged 8.2 ± 3.6 mm/min in controls (first HSD, $n = 16$), and did not differ in stress slices, nor was it affected by repeated hypoxia (**Figure 4E**). Also the relative area of the hippocampal formation invaded by HSD, i.e., the maximum spread of the reflectance increase at the height of HSD ($57.7 \pm 15.2\%$, first HSD control slice, $n = 16$), did not differ among the two groups during repeated hypoxia (**Figures 4A,F**).

SYNAPTIC FUNCTION DURING HYPOXIA/REOXYGENATION

Next, we asked whether the time course of synaptic failure during hypoxia or posthypoxic recovery differs between control and stress slices. As part of the DC potential recordings, fEPSPs were evoked every 20 s, and alterations in their amplitudes analyzed. Upon O_2 withdrawal, fEPSP amplitudes rapidly declined to 50% of their original (prehypoxic) amplitude within 60 s of hypoxia, and synaptic function was lost completely within 120 s. This time course of synaptic failure was identical in control ($n = 24$) and stress slices ($n = 28$; **Figure 5**). Clear differences became apparent, however, during the posthypoxic recovery of synaptic function. In controls, fEPSP amplitudes slowly recovered regaining 50% responses within 6.7 min of reoxygenation. In contrast, in stress slices recovery was markedly slower; on average, 50% fEPSP amplitudes were reached only after 9.7 min of reoxygenation (see arrow marks in **Figure 5**). Within the 20 min of recovery monitored, synaptic responses then recovered to a stable plateau, and this final degree of recovery also tended to be less complete in stress slices (**Figure 5**).

STRESS MODULATES GFAP CONTENT AS WELL AS Kir EXPRESSION

Glial cells play a crucial role in the buffering of interstitial K^+ during periods of increased neuronal activity as well as hypoxia (Somjen, 1979; Swanson et al., 1997; Holthoff and Witte, 2000; Kofuji and Newman, 2004). We therefore asked whether the more intense changes in $[K^+]_o$ during hypoxia and HSD and the slower posthypoxic recovery could be due to a modification of glial cells by chronic restraint stress.

Immunolabeling revealed an increased GFAP immunoreactivity in hippocampal sections from stressed rats (**Figure 6A**). A more detailed analysis in the CA1 subfield confirmed that in sections of stressed rats, the relative optical density of GFAP labeling was significantly increased by an average of 36.9% (*st. oriens*) and 38.4% (*st. radiatum)*, as compared to controls (control $n = 12$, stress $n = 27$; **Figure 6A**). Furthermore, counting the number of reactive astrocytes revealed a significant increase in the number of GFAP-positive cells within CA1 *st. radiatum* of stressed rats (577 ± 87 cells/mm^2) as compared to controls (469 ± 81 cell/mm^2; $n = 12$ sections each). At the same time, the hippocampi of stressed rats were apparently smaller than those of the controls. Comparing the areas of the hippocampal formation in the sections (control $n = 10$, stress $n = 13$) indicated an average area reduction by 13.1% in stressed rats.

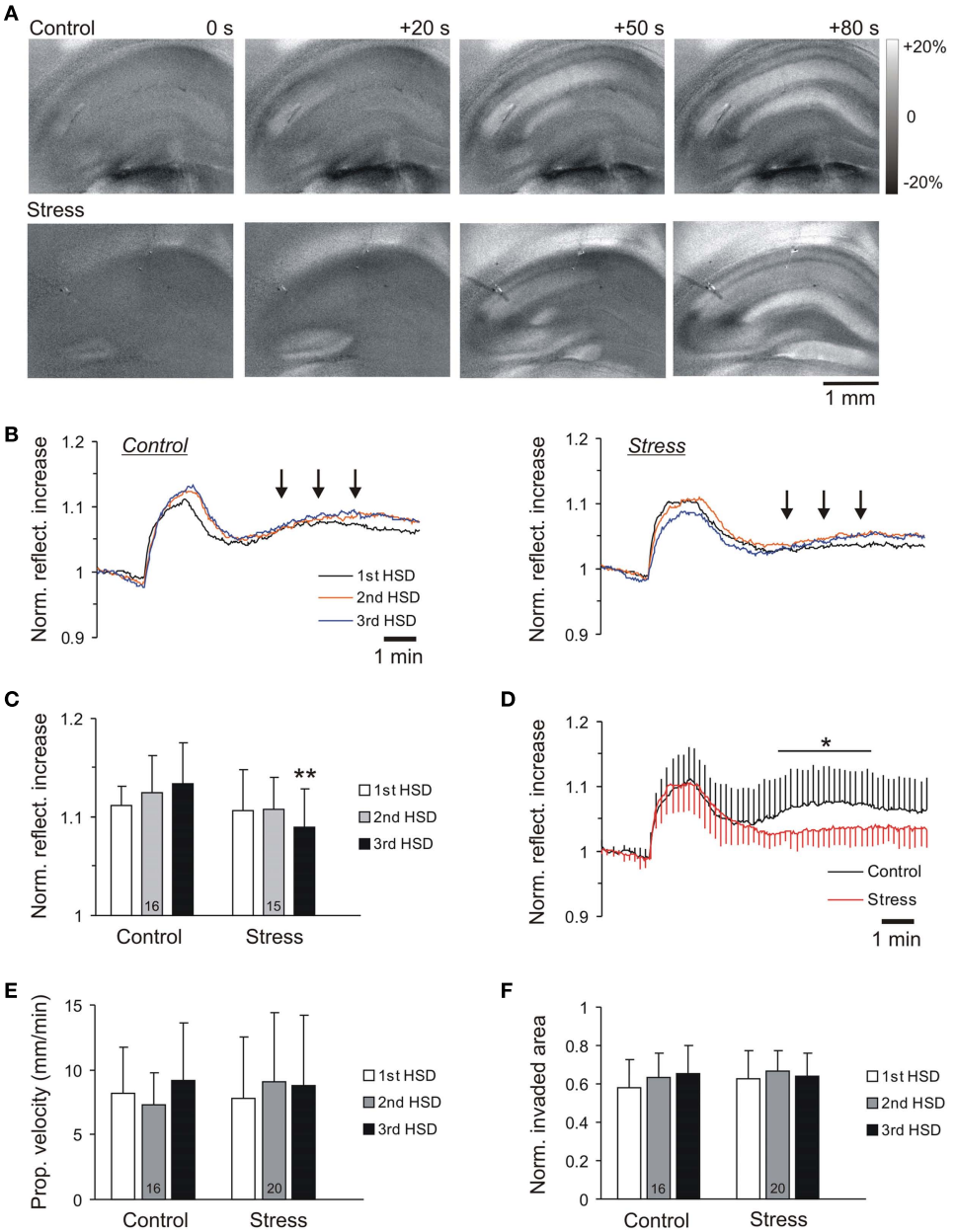

FIGURE 4 | Intrinsic optical signal analyses define the spatiotemporal pattern of HSD propagation. (A) Subtraction images of the changes in tissue reflectance visualizing the propagation of HSD within the hippocampal subfield. Numbers report the time since occurrence of the first optical changes ($t = 0$) and the last image shows the maximum spatial spread of HSD. The reflectance changes are coded in a gray-scale covering a range of ±20% as referred to prehypoxic baseline. **(B)** Time course of the reflectance changes in control and stress slices. Neither the kinetics nor the intensity of the scattering increase reveal marked changes among the two groups. Plotted are the averages of 16 control and 15 stress slices for the first, second, and third hypoxic episode; for clarity, error bars were omitted. **(C)** Quantification of the reflectance increase shows only a trend of a somewhat reduced intensity at the height of HSD for stress slices, which reaches the level of significance only for the third hypoxic episode. **(D)** During posthypoxic recovery, control slices showed a moderate secondary reflectance increase [see also arrow marks in **(B)**] which was absent in stress slices. For clarity, error bars are shown for every 5th data point only; the range of significant changes is marked. **(E)** The propagation velocity of the HSD wave front does not differ in control and stress slices during the three hypoxic episodes. **(F)** Normalized tissue invasion reports the maximum spread of HSD within the hippocampal formation. Differences were not observed among control and stress slices.

As earlier reports demonstrated that Kir channels contribute to glial K^+ uptake in spatial buffering (Neusch et al., 2006; Djukic et al., 2007; Seifert et al., 2009; Chever et al., 2010), we screened for an altered expression of this glial (astrocyte)-specific channel (Tang et al., 2009). Indeed, immunolabeling revealed a clearly reduced Kir4.1 immunoreactivity in the CA1 subfield of stressed

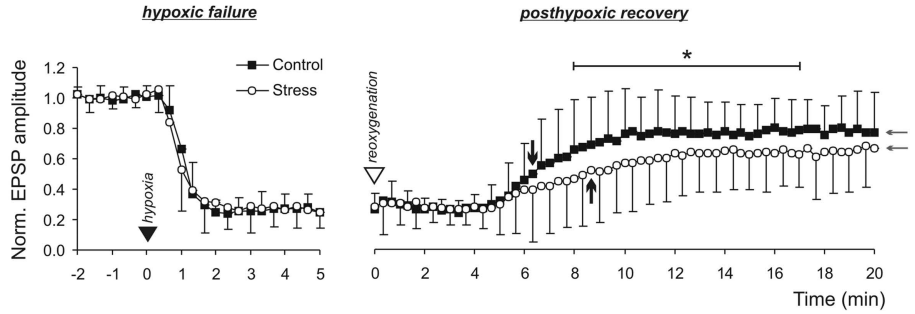

FIGURE 5 | Hypoxia-induced failure of synaptic function and posthypoxic recovery. Synaptic function is lost within 1–2 min upon O_2 withdrawal (filled triangle mark) in control and stress slices. Upon reoxygenation (open triangle mark), recovery of synaptic function is slower in stress slices. The time points at which the fEPSPs regained 50% of their normoxic amplitudes are marked by the black arrows. Furthermore, the final degree of recovery tended to be less complete in stress ($n = 28$) than in control slices ($n = 24$; see gray arrows). Since the semi-automated analysis of fEPSPs amplitudes detected noise peaks within the traces, zero-amplitudes were not quite reached during hypoxia. Nevertheless, in the raw traces, detectable fEPSPs were absent upon stimulation.

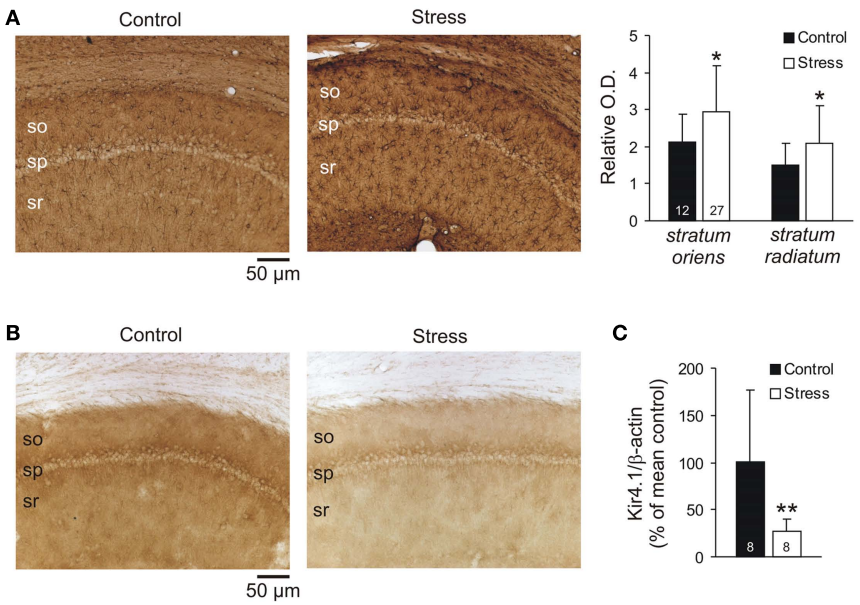

FIGURE 6 | Quantification of GFAP and Kir4.1 expression. **(A)** Immunolabeling of the astrocytic marker GFAP revealed an increased GFAP immunoreactivity in the hippocampal CA1 subfield in sections from stressed rats. Relative optical density of the sections was determined in *st. oriens* and *st. radiatum* (bar plots on the right). In both layers, GFAP immunoreactivity was more dense in stressed as compared to control rats. The number of sections analyzed is reported (so *st. oriens*, sp *st. pyramidale*, sr *st. radiatum*). **(B)** Immunolabeling also revealed a downregulation of Kir4.1 in stressed rats that was obvious in all layers of the CA1 subfield. **(C)** Western blots confirmed the decreased Kir4.1 immunoreactivity, yielding a decreased expression of Kir4.1 as compared to β-actin content in stressed rats ($n = 8$ hippocampi each group).

rats (**Figure 6B**). This downregulation of Kir4.1 protein was confirmed by Western blot analyses of whole hippocampi ($n = 8$ each group, **Figure 6C**).

DOES STRESS IMPAIR GLIAL K^+-BUFFERING?

Especially the changes in $[K^+]_o$ during the early period of hypoxia are considered to be shaped by glial K^+ buffering. In view of the confirmed downregulation of Kir4.1, we therefore addressed the possibility that the rate and/or capacity of astroglial K^+ uptake might be attenuated in stressed rats and performed whole-cell voltage-clamp recordings from CA1 astrocytes. For unequivocal identification, astrocytes were labeled with SR101 (1 µM, 20 min bulk loading of slices; **Figure 7A**). Against expectation, the resting membrane potential of astrocytes did not differ significantly between control and stress slices (-66 ± 6.8 mV $n = 14$ and -70.5 ± 7.6 mV $n = 12$, respectively; **Figure 7B**). The membrane resistance (R_i), although quite variable, was not affected either (control 72.7 ± 35.3 MΩ $n = 14$, stress 92.8 ± 98.7 MΩ $n = 12$; **Figure 7B**). Neither did the IV-curve, which was determined by a voltage step protocol, show any differences (**Figures 7C,D**).

To test for functional differences of K^+ channels in astrocytes of control and stressed rats, hippocampal slices were exposed to

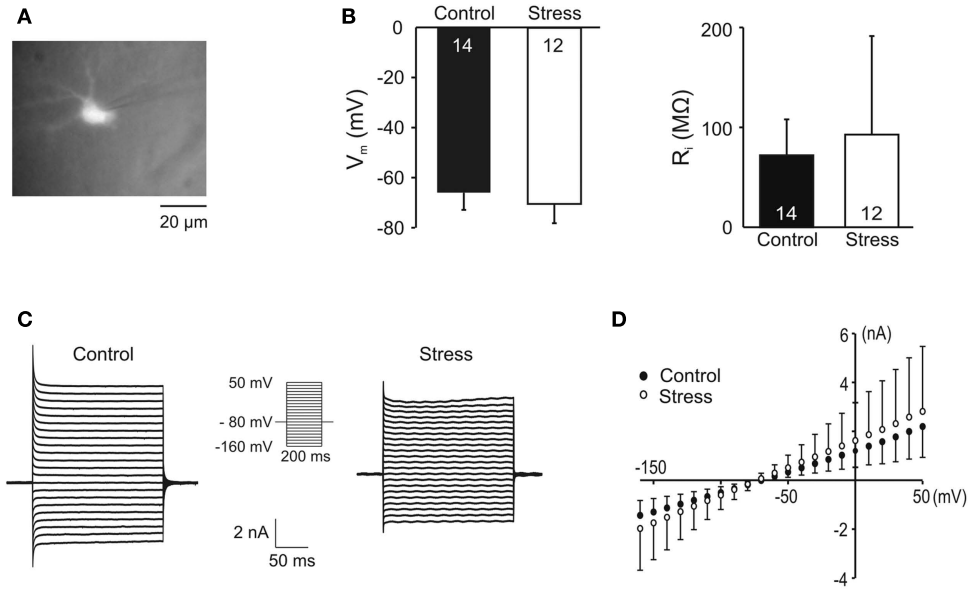

FIGURE 7 | Electrophysiological analyses of hippocampal glial cells. **(A)** *St. radiatum* astrocytes were identified by labeling with the astrocyte-specific fluorescent marker sulforhodamine101. **(B)** The resting membrane potential (V_m) and input resistance (R_i) of astrocytes did not differ among control and stress slices. **(C)** Whole-cell current responses of astrocytes to voltage steps from −80 mV holding potential to various test potentials ranging from −160 to +50 mV in 10 mV increments (see insert). **(D)** Summarized IV-curves of astrocytes from control and stress slices.

elevated K^+ levels (50 mM; **Figure 8**). This treatment evokes a K^+-mediated inward current (I_K) in astrocytes which apparently requires Kir4.1 channels (Neusch et al., 2006). However, there were no obvious differences in the K^+-evoked I_K currents in astrocytes of control and stress slices, with amplitudes averaging -1.6 ± 0.8 and -2.5 ± 1.6 nA, respectively. Furthermore, there was no change in the K^+-induced increase of the inward current (ΔI_{-160}) that was elicited by a voltage step from −80 to −160 mV (control -2.8 ± 1.7 nA, stress -3.8 ± 2.4 nA; **Figure 8**).

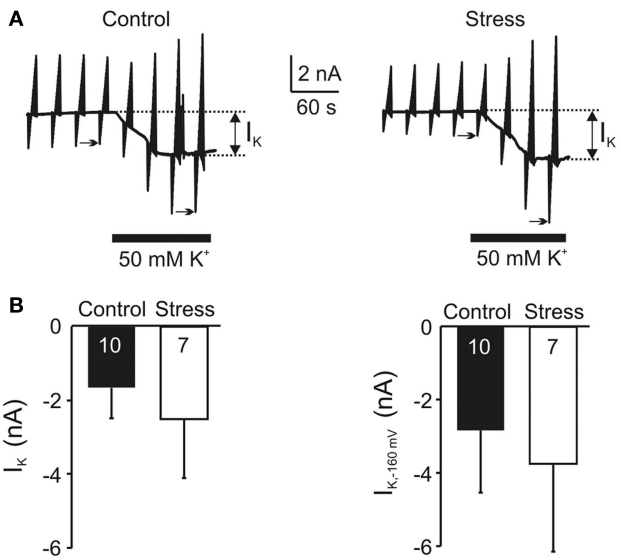

FIGURE 8 | Quantification of K^+ fluxes in astrocytes. **(A)** Voltage-clamp recordings of *st. radiatum* astrocytes ($V_{hold} = -80$ mV) that were repetitively subjected to defined voltage step protocols (see **Figure 7C**). Application of 50 mM K^+ elicited an inward current (I_K, see arrows) of similar amplitude in astrocytes from control and stress slices. **(B)** Statistical comparison of the 50 mM K^+-mediated inward current (I_K) and potentiation of that current by hyperpolarizing voltage steps from −80 to −160 mV [ΔI_{-160}; see arrow marks in **(A)**].

DISCUSSION

Chronic restraint stress was induced following an established protocol. The confirmed reduced body weight gain and the increased relative adrenal weight indicate hyperactivity of the hypothalamus–pituitary adrenal axis and thus confirm that the stress procedure was effective (Watanabe et al., 1992). In a multiparametric approach we have analyzed the consequences of chronic stress on the hippocampal network functioning. In slices from stressed animals we analyzed the responses to severe hypoxia, and detected clear differences as compared to control animals. In stressed rats, changes in the interstitial K^+ levels during the early phase of hypoxia were more intense, the HSD-associated DC potential shift was shortened, the postsynaptic recovery of the interstitial K^+ level was slower, and synaptic function was impaired more severely. Furthermore, immunolabeling revealed pronounced changes in glial cells, i.e., an increased number of GFAP-positive astrocytes and a reduced expression of Kir4.1 channels.

IMPACT ON SYNAPTIC AND NETWORK FUNCTION

In stress slices, basal synaptic function was intact. Also PPF, a measure of short-term plasticity due to presynaptically altered transmitter release (Kuhnt and Voronin, 1994) was unchanged, which is in line with earlier observations after acute restraint stress

(Shors and Thompson, 1992). In addition, the stress-induced inhibition of hippocampal LTP is in agreement with previous reports (Pavlides et al., 2002). We found that induction of LTP caused an indistinguishable immediate PTP in control and stress slices, but about 10 min after initiation, this potentiation slowly faded in stress slices so that an induction and maintenance of stable LTP did not occur. Therefore, in terms of synaptic plasticity, chronic restraint stress can be assumed to target primarily postsynaptic processes. Whether a more pronounced interstitial K^+ accumulation has also occurred in response to the LTP-inducing high-frequency stimulus cannot be decided, as $[K^+]_o$ was not recorded during these experiments.

The impact of stress and the associated increase in corticosteroid levels on synaptic function and plasticity is quite heterogeneous. It depends on the very brain region with its particular synapses/neuropil, and especially the type of stress that is applied as well as on the stress duration (Pavlides et al., 2002). For example, a suppression of LTP within *st. radiatum* of the CA1 subfield was reported in response to acute stress while leaving basal synaptic function and PPF intact (Shors and Thompson, 1992; Fujikawa et al., 1996). Also corticosterone treatment or activation of specific glucocorticoid receptors dose-dependently dampened LTP in the CA1 region (Kerr et al., 1994). An inverted-U shape relationship between peripheral corticosterone levels and hippocampal primed burst potentiation was detected in rats whose glucocorticoid levels were modulated by adrenalectomy and exogenous corticosterone, respectively (Diamond et al., 1992). However, whereas acute stress or low corticosteroids may even facilitate and improve synaptic plasticity, there is a general agreement that chronic stress mediates suppressive effects (Bodnoff et al., 1995; Pavlides et al., 2002). Our present findings support this view as the chronic restraint stress suppressed LTP in the CA1 subfield.

To some degree, the neuronal functioning was probably altered because of stress-induced changes in the neuronal architecture. Chronic restraint stress reduces the length of apical dendrites in the CA3 subfield which may also affect CA1 neurons, although no such morphological alterations were detected in CA1 itself (see Watanabe et al., 1992). However, the Schaffer collateral mediated input to the CA1 subfield is dependent on the activation of NMDA receptors (Collingridge and Bliss, 1995). In earlier studies it was suggested that the suppression of synaptic plasticity by adrenal steroids and stress includes changes in NMDA receptors (Fujikawa et al., 1996; Pavlides et al., 2002). This may be related to high extracellular glutamate levels in the hippocampus induced by stress or glucocorticoid treatment (Lowy et al., 1993; Moghaddam et al., 1994). Chronic stress has been shown to affect the clearance of extracellular glutamate (for review see Popoli et al., 2012). Acute restraint stress enhanced both glutamate release and uptake in hippocampal synaptosomes (Gilad et al., 1990), and the NMDA receptor subunit NR1 was found to be upregulated in rat hippocampus upon restraint stress (Jang et al., 2008). Altogether, such changes in the glutamatergic system could lead to altered NMDA receptor functioning and hence to an impairment of LTP. Furthermore, altered NMDA receptor function could have well contributed to the observed changes in the HSD-associated DC potential shift (see below).

Another interesting observation is the delayed recovery of synaptic function in stress slices upon reoxygenation. A variety of mechanisms contributes to the synaptic failure during hypoxia, including inhibition of presynaptic voltage-gated Ca^{2+} channels (Young and Somjen, 1992) as well as activation of various pre- and post-synaptic ATP- and Ca^{2+}-sensitive or adenosine-mediated K^+ conductances (Luhmann and Heinemann, 1992; Zhu and Krnjevic, 1997; Nowicky and Duchen, 1998). Only if O_2 is restored in time, synaptic function eventually recovers once the massively disturbed ionic homeostasis and resting membrane potentials have been largely normalized. The delayed posthypoxic recovery of synaptic function in stress slices suggests that this normalization of membrane potentials and ionic distribution took somewhat longer. Of course a more detailed interpretation would require intracellular recordings from individual neurons, but the observed slower posthypoxic recovery of $[K^+]_o$ in stress slices provides strong evidence for a delayed reinstatement of neuronal resting membrane potentials and hence a plausible cause for the postponed recovery of synaptic function.

CHRONIC STRESS INDUCES GLIAL CHANGES

Several stress-induced changes in glia may exert crucial effects on network function. The increase in the number of GFAP immunoreactive astrocytes is in line with previous findings indicating a reactive gliosis, accompanied by an increase in glial volume and hence a reduction of interstitial space (Jang et al., 2008). The present increase in the number of GFAP-positive cells strongly suggests that such a reduction of interstitial volume has also occurred within the hippocampal formation in our study. This view is further supported by the finding that the size of the hippocampus of stressed rats appeared smaller than that of the controls.

MODULATION OF HSD AND ITS SPATIOTEMPORAL PROPAGATION PATTERN

High-frequency stimulation induces epileptic afterdischarges in the CA3 subfield in acutely stressed and less regularly also in chronically stressed rats (Pavlides et al., 2002). A similar hyperexcitability in CA1 neurons as a result of chronic stress can be excluded. In our experiments, fEPSPs did not show clear signs of hyperexcitability such as multiple population spikes or afterdischarges, and the input–output curve was not shifted to the left. Also, an increase in neuronal excitability should have hastened the occurrence of HSD, as neuronal excitability is one of the key parameters defining the susceptibility of brain tissue to the generation of HSD (Aitken et al., 1991; Müller, 2000; Müller and Somjen, 2000b). Furthermore, IOS monitoring confirmed a comparable spatiotemporal profile of HSD in the hippocampal formation of control and stress slices.

It has been reported that stress stimulates the production of nitric oxide via activation of the inducible nitric oxide synthase and it was proposed that this may result in neurodegenerative changes within the hippocampal formation (Jang et al., 2008). However, clear evidence for the loss of neurons was never obtained. We subjected the rats to daily restraint stress according to a protocol that is widely used to study chronic stress effects on the brain. This daily immobilization induces a kind of psychological stress leading to various morphological/biochemical changes in neurons,

e.g., the retraction of hippocampal pyramidal neuron dendrites. Yet, despite the popular view that psychological stress induces neuronal death in the hippocampus this phenomenon was never observed under controlled experimental conditions (Fuchs et al., 2004). Instead, several of the stress-induced changes in the brain, e.g., the retraction of hippocampal dendrites and the reduced neurogenesis rate in dentate gyrus, are reversible, at least when the animals are treated with antidepressant drugs (McEwen et al., 2002). Moreover, in another established chronic stress model, the male tree shrew, the exact quantification of hippocampal neurons confirmed that there was no neuron loss (Vollmann-Honsdorf et al., 1997). Instead, chronic (psychological) stress may even reduce apoptosis in certain hippocampal regions (Lucassen et al., 2001).

Neither do our data show any obvious signs of neurodegeneration. Basal synaptic function (fEPSPs) and short-term plasticity (PPF and PTP) were intact, and the time to onset of HSD and its spatiotemporal propagation pattern were unchanged. Since HSD is generated and propagates in healthy brain tissue (gray matter) only, the largely unaltered electrophysiological and optical characteristics of HSD further argue against neurodegeneration. Accordingly, the present findings showing that stress changes hippocampal neurons in their capacity to react to hypoxia is in line with the view that stress *per se* has profound effects on neuronal physiology but does not kill brain cells (see also Fuchs and Flügge, 2011). Of course, this interpretation does not exclude that an *in vivo* hypoxic or toxic insult could have stronger degenerating effects on neurons in stressed subjects as compared to controls.

The shortened duration of the DC potential shift is an interesting observation which could be explained by an improved synchronization of the underlying neuronal/glial depolarizations, possibly as a cause of the faster K^+ accumulation which should render neurons more excitable. Another plausible explanation might be based on the fact that also the shape of the DC potential shift was altered. Under control conditions, the profile of the DC shift often showed the characteristic "inverted saddle" shape with an initial nadir followed by a second negative peak (e.g., **Figure 2B**). It is well known that these two negative peaks are based on the contribution of different types of ionotropic glutamate receptors, with NMDA receptor-mediated currents contributing markedly to the second peak (Marrannes et al., 1988; Herreras and Somjen, 1993; Krüger et al., 1999). Due to the above mentioned effects of chronic stress on NMDA receptor function and dendritic complexity, a reduced availability of functional NMDA receptors would be a plausible explanation for the characteristic alterations in the DC potential profile and hence the shorting of its duration.

A reduced complexity of dendritic structures is also a likely explanation for the observed depression of the secondary reflectance increase in stress slices upon reoxygenation, because these late components of the IOS are considered to arise – at least in part – from alterations in dendritic morphology such as beading and swelling (Andrew et al., 1999; Müller and Mané, 2010). Any other alterations in the time course of the IOS were not observed, and cannot be expected. The shortening of the DC potential shift in stress slices was only moderate and the IOS would only be affected by pronounced changes in HSD duration, such as a markedly delayed reoxygenation (Gerich et al., 2006).

MODULATION OF HYPOXIC K^+ FLUXES

Early during hypoxia, $[K^+]_o$ rose at a higher rate and reached a higher level before HSD was ignited. The K^+ peak at the height of HSD also became intensified in stressed rats, at least when HSD was induced repeatedly, and the posthypoxic recovery of $[K^+]_o$ occurred more slowly. These more pronounced changes in $[K^+]_o$ could be based on three different causes or any combination thereof: (1) more intense release of K^+ from stress neurons, (2) limited degree of K^+ buffering by stress glial cells, and (3) a reduced interstitial volume in stressed rats.

Clear signs of hyperexcitability were absent in stressed rats, and the time course of synaptic failure was indistinguishable among control and stress slices. Furthermore, the early hyperpolarization of hippocampal CA1 neurons during hypoxia is already quite pronounced and drives the membrane potential close to the K^+ equilibrium potential (Hansen et al., 1982; Fujimura et al., 1997; Müller and Somjen, 2000a). Therefore, a more pronounced release of K^+ from hippocampal neurons is rather unlikely.

An interesting aspect is a modulation of glial K^+ uptake, especially in view of the altered GFAP expression indicating reactive gliosis and the downregulation of Kir4.1 protein. Based on findings in Kir4.1 knock-out mice, we expected that the strongly reduced expression of Kir4.1 in stressed rats would result in a more depolarized astroglial resting membrane potential and decreased K^+-induced inward currents in astrocytes (Neusch et al., 2006; Djukic et al., 2007). However, astrocytes from stressed rats did not show any of those changes reported for Kir4.1 deficient mice. It is well possible that in stressed rats, the remaining Kir4.1 protein, in concert with other K^+ channels (Seifert et al., 2009), was able to maintain the resting membrane potential and K^+ uptake capability of the astrocytes. Also, compensatory alterations by other types of K^+ channels may have occurred, masking the partial Kir4.1 loss. For example, in reactive gliosis, upregulation of astroglial TreK-1 passive K^+ channels was reported (Wang et al., 2012), preventing an observation of those changes in passive membrane properties found in other disease models with GFAP upregulation (Bordey et al., 2001; Anderova et al., 2004). Accordingly, the situation in stressed rats rather resembles those conditions found in heterozygous Kir4.1$^{+/-}$ mice, in which neither resting membrane potential nor K^+ uptake were affected (Neusch et al., 2006; Papadopoulos et al., 2008).

Since controlled whole-cell recordings from unlabeled astrocytes in slices of adult rats are almost impossible, we used SR101 to specifically label astrocytes (Kafitz et al., 2008). This labeling procedure might have biased our selection of cells to a distinct subpopulation of astroglial cells because in juvenile rat hippocampus (after P15), SR101 labels preferentially the passive type of astrocyte but not necessarily also the complex type (Kafitz et al., 2008). In a conditional, glia-specific Kir4.1 knock-out mouse, however, in particular the complex type of astrocyte shows a pronounced reduction of Kir-mediated inward currents (Djukic et al., 2007).

Nevertheless, activation of astroglia (indicated by enhanced GFAP levels) suggests an increased degree of ramification and

formation of glial processes. This could result in a restriction of the interstitial volume – especially in view of the increased number of GFAP-positive cells and the reduced size of the hippocampal formation detected in stressed rats. Thus the K^+ being released from neurons during the early phase of hypoxia would enter a more restricted interstitial volume, thereby rising at a faster rate and reaching higher levels, both of which was seen in the $[K^+]_o$ recordings. The diffusional limitations arising from the restricted interstitial volume could also explain why the posthypoxic recovery of the massive K^+ rise was slowed down in stressed rats.

Based on the available data, and in view of the unchanged electrophysiological properties of hippocampal astrocytes the alterations in extracellular K^+ accumulation and postsynaptic recovery are probably due to a restriction of the interstitial volume in the hippocampus of stressed rats rather than caused by an impaired glial K^+ uptake. Nevertheless, together with the delayed posthypoxic recovery of synaptic function, this confirms a more severe impact of O_2 shortage in neuronal networks that had been exposed to chronic stress.

ACKNOWLEDGMENTS

This study was supported by grants of the Deutsche Forschungsgemeinschaft (DFG Research Center Molecular Physiology of the Brain). We thank Cornelia Heckmann and Anja Grützner for excellent technical assistance.

REFERENCES

Aitken, P. G., Fayuk, D., Somjen, G. G., and Turner, D. A. (1999). Use of intrinsic optical signals to monitor physiological changes in brain tissue slices. *Methods* 18, 91–103.

Aitken, P. G., Jing, J., Young, J., and Somjen, G. G. (1991). Ion channel involvement in hypoxia-induced spreading depression in hippocampal slices. *Brain Res.* 541, 7–11.

Anderova, M., Antonova, T., Petrik, D., Neprasova, H., Chvatal, A., and Sykova, E. (2004). Voltage-dependent potassium currents in hypertrophied rat astrocytes after a cortical stab wound. *Glia* 48, 311–326.

Andrew, R. D., Jarvis, C. R., and Obeidat, A. S. (1999). Potential sources of intrinsic optical signals imaged in live brain slices. *Methods* 18, 185–196, 179.

Benes, F. M., Parks, T. N., and Rubel, E. W. (1977). Rapid dendritic atrophy following deafferentation: an EM morphometric analysis. *Brain Res.* 122, 1–13.

Bodnoff, S. R., Humphreys, A. G., Lehman, J. C., Diamond, D. M., Rose, G. M., and Meaney, M. J. (1995). Enduring effects of chronic corticosterone treatment on spatial learning, synaptic plasticity, and hippocampal neuropathology in young and mid-aged rats. *J. Neurosci.* 15, 61–69.

Bordey, A., Lyons, S. A., Hablitz, J. J., and Sontheimer, H. (2001). Electrophysiological characteristics of reactive astrocytes in experimental cortical dysplasia. *J. Neurophysiol.* 85, 1719–1731.

Buwalda, B., Kole, M. H., Veenema, A. H., Huininga, M., De Boer, S. F., Korte, S. M., and Koolhaas, J. M. (2005). Long-term effects of social stress on brain and behavior: a focus on hippocampal functioning. *Neurosci. Biobehav. Rev.* 29, 83–97.

Chever, O., Djukic, B., Mccarthy, K. D., and Amzica, F. (2010). Implication of Kir4.1 channel in excess potassium clearance: an in vivo study on anesthetized glial-conditional Kir4.1 knock-out mice. *J. Neurosci.* 30, 15769–15777.

Clarke, D. D., Nicklas, W. J., and Berl, S. (1970). Tricarboxylic acid-cycle metabolism in brain. Effect of fluoroacetate and fluorocitrate on the labelling of glutamate, aspartate, glutamine and gamma-aminobutyrate. *Biochem. J.* 120, 345–351.

Collingridge, G. L., and Bliss, T. V. (1995). Memories of NMDA receptors and LTP. *Trends Neurosci.* 18, 54–56.

Czéh, B., Abumaria, N., Rygula, R., and Fuchs, E. (2010). Quantitative changes in hippocampal microvasculature of chronically stressed rats: no effect of fluoxetine treatment. *Hippocampus* 20, 174–185.

Czéh, B., Simon, M., Schmelting, B., Hiemke, C., and Fuchs, E. (2006). Astroglial plasticity in the hippocampus is affected by chronic psychosocial stress and concomitant fluoxetine treatment. *Neuropsychopharmacology* 31, 1616–1626.

Deitch, J. S., and Rubel, E. W. (1984). Afferent influences on brain stem auditory nuclei of the chicken: time course and specificity of dendritic atrophy following deafferentation. *J. Comp. Neurol.* 229, 66–79.

Diamond, D. M., Bennett, M. C., Fleshner, M., and Rose, G. M. (1992). Inverted-U relationship between the level of peripheral corticosterone and the magnitude of hippocampal primed burst potentiation. *Hippocampus* 2, 421–430.

Djukic, B., Casper, K. B., Philpot, B. D., Chin, L. S., and Mccarthy, K. D. (2007). Conditional knock-out of Kir 4.1 leads to glial membrane depolarization, inhibition of potassium and glutamate uptake, and enhanced short-term synaptic potentiation. *J. Neurosci.* 27, 11354–11365.

Dodt, H. U., and Zieglgänsberger, W. (1994). Infrared videomicroscopy: a new look at neuronal structure and function. *Trends Neurosci.* 17, 453–458.

Fayuk, D., Aitken, P. G., Somjen, G. G., and Turner, D. A. (2002). Two different mechanisms underlie reversible, intrinsic optical signals in rat hippocampal slices. *J. Neurophysiol.* 87, 1924–1937.

Fischer, M., Reuter, J., Gerich, F. J., Hildebrandt, B., Hägele, S., Katschinski, D., and Müller, M. (2009). Enhanced hypoxia susceptibility in hippocampal slices from a mouse model of Rett syndrome. *J. Neurophysiol.* 101, 1016–1032.

Fuchs, E., Czéh, B., Kole, M. H., Michaelis, T., and Lucassen, P. J. (2004). Alterations of neuroplasticity in depression: the hippocampus and beyond. *Eur. Neuropsychopharmacol.* 14(Suppl. 5), S481–S490.

Fuchs, E., and Flügge, G. (2011). "Chronic stress and depression," in *The Handbook of Stress: Neuropsychological Effects on the Brain*, ed. C. D. Conrad (New York: Blackwell Publishing), 463–479.

Fuchs, E., Flügge, G., and Czéh, B. (2006). Remodeling of neuronal networks by stress. *Front. Biosci.* 11, 2746–2758.

Fujikawa, D. G., Kim, J. S., Daniels, A. H., Alcaraz, A. F., and Sohn, T. B. (1996). In vivo elevation of extracellular potassium in the rat amygdala increases extracellular glutamate and aspartate and damages neurons. *Neuroscience* 74, 695–706.

Fujimura, N., Tanaka, E., Yamamoto, S., Shigemori, M., and Higashi, H. (1997). Contribution of ATP-sensitive potassium channels to hypoxic hyperpolarization in rat hippocampal CA1 neurons in vitro. *J. Neurophysiol.* 77, 378–385.

Gerich, F. J., Hepp, S., Probst, I., and Müller, M. (2006). Mitochondrial inhibition prior to oxygen-withdrawal facilitates the occurrence of hypoxia-induced spreading depression in rat hippocampal slices. *J. Neurophysiol.* 96, 492–504.

Gilad, G. M., Gilad, V. H., Wyatt, R. J., and Tizabi, Y. (1990). Region-selective stress-induced increase of glutamate uptake and release in rat forebrain. *Brain Res.* 525, 335–338.

Golding, N. L., Kath, W. L., and Spruston, N. (2001). Dichotomy of action-potential backpropagation in CA1 pyramidal neuron dendrites. *J. Neurophysiol.* 86, 2998–3010.

Gorji, A. (2001). Spreading depression: a review of the clinical relevance. *Brain Res. Brain Res. Rev.* 38, 33–60.

Hansen, A. J. (1985). Effect of anoxia on ion distribution in the brain. *Physiol. Rev.* 65, 101–148.

Hansen, A. J., Hounsgaard, J., and Jahnsen, H. (1982). Anoxia increases potassium conductance in hippocampal nerve cells. *Acta Physiol. Scand.* 115, 301–310.

Hassel, B., Paulsen, R. E., Johnsen, A., and Fonnum, F. (1992). Selective inhibition of glial cell metabolism in vivo by fluorocitrate. *Brain Res.* 576, 120–124.

Hepp, S., Gerich, F. J., and Müller, M. (2005). Sulfhydryl oxidation reduces hippocampal susceptibility to hypoxia-induced spreading depression by activating BK-channels. *J. Neurophysiol.* 94, 1091–1103.

Hepp, S., and Müller, M. (2008). Sulfhydryl oxidation: a potential strategy to achieve neuroprotection during severe hypoxia? *Neuroscience* 152, 903–912.

Herreras, O., and Somjen, G. G. (1993). Analysis of potential shifts associated with recurrent spreading depression and prolonged unstable spreading depression induced by microdialysis of elevated K^+ in hippocampus of anesthetized rats. *Brain Res.* 610, 283–294.

Holthoff, K., and Witte, O. W. (2000). Directed spatial potassium redistribution in rat neocortex. *Glia* 29, 288–292.

Jang, S., Suh, S. H., Yoo, H. S., Lee, Y. M., and Oh, S. (2008). Changes in iNOS, GFAP and NR1 expression in various brain regions and elevation of sphingosine-1-phosphate in serum after immobilized stress. *Neurochem. Res.* 33, 842–851.

Kafitz, K. W., Meier, S. D., Stephan, J., and Rose, C. R. (2008). Developmental profile and properties of sulforhodamine 101-labeled glial cells in acute brain slices of rat hippocampus. *J. Neurosci. Methods* 169, 84–92.

Kerr, D. S., Huggett, A. M., and Abraham, W. C. (1994). Modulation of hippocampal long-term potentiation and long-term depression by corticosteroid receptor activation. *Psychobiology* 22, 123–133.

Kofuji, P., and Newman, E. A. (2004). Potassium buffering in the central nervous system. *Neuroscience* 129, 1045–1056.

Kole, M. H., Czéh, B., and Fuchs, E. (2004). Homeostatic maintenance in excitability of tree shrew hippocampal CA3 pyramidal neurons after chronic stress. *Hippocampus* 14, 742–751.

Kossel, A. H., Williams, C. V., Schweizer, M., and Kater, S. B. (1997). Afferent innervation influences the development of dendritic branches and spines via both activity-dependent and non-activity-dependent mechanisms. *J. Neurosci.* 17, 6314–6324.

Krüger, H., Heinemann, U., and Luhmann, H. J. (1999). Effects of ionotropic glutamate receptor blockade and 5-HT1A receptor activation on spreading depression in rat neocortical slices. *Neuroreport* 10, 2651–2656.

Kuhnt, U., and Voronin, L. L. (1994). Interaction between paired-pulse facilitation and long-term potentiation in area CA1 of guinea-pig hippocampal slices: application of quantal analysis. *Neuroscience* 62, 391–397.

Largo, C., Cuevas, P., Somjen, G. G., Martin Del Rio, R., and Herreras, O. (1996). The effect of depressing glial function in rat brain in situ on ion homeostasis, synaptic transmission, and neuron survival. *J. Neurosci.* 16, 1219–1229.

Largo, C., Ibarz, J. M., and Herreras, O. (1997). Effects of the gliotoxin fluorocitrate on spreading depression and glial membrane potential in rat brain in situ. *J. Neurophysiol.* 78, 295–307.

Lauritzen, M., Dreier, J. P., Fabricius, M., Hartings, J. A., Graf, R., and Strong, A. J. (2011). Clinical relevance of cortical spreading depression in neurological disorders: migraine, malignant stroke, subarachnoid and intracranial hemorrhage, and traumatic brain injury. *J. Cereb. Blood Flow Metab.* 31, 17–35.

Leão, A. A. P. (1947). Further observations on the spreading depression of activity in the cerebral cortex. *J. Neurophysiol.* 10, 409–414.

Lowy, M. T., Gault, L., and Yamamoto, B. K. (1993). Adrenalectomy attenuates stress-induced elevations in extracellular glutamate concentrations in the hippocampus. *J. Neurochem.* 61, 1957–1960.

Lucassen, P. J., Vollmann-Honsdorf, G. K., Gleisberg, M., Czéh, B., De Kloet, E. R., and Fuchs, E. (2001). Chronic psychosocial stress differentially affects apoptosis in hippocampal subregions and cortex of the adult tree shrew. *Eur. J. Neurosci.* 14, 161–166.

Luhmann, H. J., and Heinemann, U. (1992). Hypoxia-induced functional alterations in adult rat neocortex. *J. Neurophysiol.* 67, 798–811.

Magariños, A. M., and McEwen, B. S. (1995). Stress-induced atrophy of apical dendrites of hippocampal CA3c neurons: comparison of stressors. *Neuroscience* 69, 83–88.

Magariños, A. M., McEwen, B. S., Flügge, G., and Fuchs, E. (1996). Chronic psychosocial stress causes apical dendritic atrophy of hippocampal CA3 pyramidal neurons in subordinate tree shrews. *J. Neurosci.* 16, 3534–3540.

Magariños, A. M., Verdugo, J. M., and McEwen, B. S. (1997). Chronic stress alters synaptic terminal structure in hippocampus. *Proc. Natl. Acad. Sci. U.S.A.* 94, 14002–14008.

Marrannes, R., Willems, R., De Prins, E., and Wauquier, A. (1988). Evidence for a role of the N-methyl-D-aspartate (NMDA) receptor in cortical spreading depression in the rat. *Brain Res.* 457, 226–240.

McEwen, B. S., Magariños, A. M., and Reagan, L. P. (2002). Structural plasticity and tianeptine: cellular and molecular targets. *Eur. Psychiatry* 17(Suppl. 3), 318–330.

Moghaddam, B., Bolinao, M. L., Stein-Behrens, B., and Sapolsky, R. (1994). Glucocorticoids mediate the stress-induced extracellular accumulation of glutamate. *Brain Res.* 655, 251–254.

Müller, M. (2000). Effects of chloride transport inhibition and chloride substitution on neuron function and on hypoxic spreading-depression-like depolarization in rat hippocampal slices. *Neuroscience* 97, 33–45.

Müller, M., and Mané, M. (2010). *Spectrally Resolved Recordings of the Intrinsic Optical Signal During Hypoxia-Induced Spreading Depression*. Program No. 353.23, Neuroscience Meeting Planner. San Diego, CA: Society for Neuroscience.

Müller, M., and Somjen, G. G. (1998). Inhibition of major cationic inward currents prevents spreading depression-like hypoxic depolarization in rat hippocampal tissue slices. *Brain Res.* 812, 1–13.

Müller, M., and Somjen, G. G. (1999). Intrinsic optical signals in rat hippocampal slices during hypoxia-induced spreading depression-like depolarization. *J. Neurophysiol.* 82, 1818–1831.

Müller, M., and Somjen, G. G. (2000a). Na^+ and K^+ concentrations, extra- and intracellular voltages, and the effect of TTX in hypoxic rat hippocampal slices. *J. Neurophysiol.* 83, 735–745.

Müller, M., and Somjen, G. G. (2000b). Na^+ dependence and the role of glutamate receptors and Na^+ channels in ion fluxes during hypoxia of rat hippocampal slices. *J. Neurophysiol.* 84, 1869–1880.

Neusch, C., Papadopoulos, N., Müller, M., Maletzki, I., Winter, S. M., Hirrlinger, J., Handschuh, M., Bähr, M., Richter, D. W., Kirchhoff, F., and Hülsmann, S. (2006). Lack of the Kir4.1 channel subunit abolishes K^+ buffering properties of astrocytes in the ventral respiratory group: impact on extracellular K^+ regulation. *J. Neurophysiol.* 95, 1843–1852.

Nimmerjahn, A., Kirchhoff, F., Kerr, J. N., and Helmchen, F. (2004). Sulforhodamine 101 as a specific marker of astroglia in the neocortex in vivo. *Nat. Methods* 1, 31–37.

Nowicky, A. V., and Duchen, M. R. (1998). Changes in $[Ca2^+]_i$ and membrane currents during impaired mitochondrial metabolism in dissociated rat hippocampal neurons. *J. Physiol.* 507, 131–145.

Papadopoulos, N., Winter, S. M., Härtel, K., Kaiser, M., Neusch, C., and Hülsmann, S. (2008). Possible roles of the weakly inward rectifying K^+ channel Kir4.1 (KCNJ10) in the pre-Bötzinger complex. *Adv. Exp. Med. Biol.* 605, 109–113.

Pavlides, C., Nivon, L. G., and McEwen, B. S. (2002). Effects of chronic stress on hippocampal long-term potentiation. *Hippocampus* 12, 245–257.

Paxinos, G., and Watson, C. (1986). *The Rat Brain in Stereotaxic Coordinates.* San Diego: Academic Press Inc.

Popoli, M., Yan, Z., McEwen, B. S., and Sanacora, G. (2012). The stressed synapse: the impact of stress and glucocorticoids on glutamate transmission. *Nat. Rev. Neurosci.* 13, 22–37.

Pulsinelli, W. A., Brierley, J. B., and Plum, F. (1982). Temporal profile of neuronal damage in a model of transient forebrain ischemia. *Ann. Neurol.* 11, 491–498.

Schaefer, A. T., Larkum, M. E., Sakmann, B., and Roth, A. (2003). Coincidence detection in pyramidal neurons is tuned by their dendritic branching pattern. *J. Neurophysiol.* 89, 3143–3154.

Schmidt-Kastner, R., and Freund, T. F. (1991). Selective vulnerability of the hippocampus in brain ischemia. *Neuroscience* 40, 599–636.

Seifert, G., Huttmann, K., Binder, D. K., Hartmann, C., Wyczynski, A., Neusch, C., and Steinhäuser, C. (2009). Analysis of astroglial K^+ channel expression in the developing hippocampus reveals a predominant role of the Kir4.1 subunit. *J. Neurosci.* 29, 7474–7488.

Shors, T. J., and Thompson, R. F. (1992). Acute stress impairs (or induces) synaptic long-term potentiation (LTP) but does not affect paired-pulse facilitation in the stratum radiatum of rat hippocampus. *Synapse* 11, 262–265.

Somjen, G. G. (1979). Extracellular potassium in the mammalian central nervous system. *Annu. Rev. Physiol.* 41, 159–177.

Somjen, G. G. (2001). Mechanisms of spreading depression and hypoxic spreading depression-like depolarization. *Physiol. Rev.* 81, 1065–1096.

Swanson, R. A., Farrell, K., and Stein, B. A. (1997). Astrocyte energetics, function, and death under conditions of incomplete ischemia: a mechanism of glial death in the penumbra. *Glia* 21, 142–153.

Tang, X., Taniguchi, K., and Kofuji, P. (2009). Heterogeneity of Kir4.1 channel expression in glia revealed by mouse transgenesis. *Glia* 57, 1706–1715.

Valverde, F. (1968). Structural changes in the area striata of the mouse after enucleation. *Exp. Brain Res.* 5, 274–292.

Vollmann-Honsdorf, G. K., Flügge, G., and Fuchs, E. (1997). Chronic psychosocial stress does not affect the number of pyramidal neurons in tree shrew hippocampus. *Neurosci. Lett.* 233, 121–124.

Wang, M., Song, J., Xiao, W., Yang, L., Yuan, J., Wang, W., Yu, Z., and Xie, M. (2012). Changes in lipid-sensitive two-pore domain potassium channel TREK-1 expression and its involvement in astrogliosis following cerebral ischemia in rats. *J. Mol. Neurosci.* 46, 384–392.

Watanabe, Y., Gould, E., and McEwen, B. S. (1992). Stress induces atrophy of apical dendrites of hippocampal CA3 pyramidal neurons. *Brain Res.* 588, 341–345.

Young, J. N., and Somjen, G. G. (1992). Suppression of presynaptic calcium currents by hypoxia in hippocampal tissue slices. *Brain Res.* 573, 70–76.

Zhu, P. J., and Krnjevic, K. (1997). Adenosine release mediates cyanide-induced suppression of CA1 neuronal activity. *J. Neurosci.* 17, 2355–2364.

Conflict of Interest Statement: The authors declare that the research was conducted in the absence of any commercial or financial relationships that could be construed as a potential conflict of interest.

Received: 16 February 2012; paper pending published: 29 February 2012; accepted: 12 March 2012; published online: 28 March 2012.

*Citation: Schnell C, Janc OA, Kempkes B, Callis CA, Flügge G, Hülsmann S and Müller M (2012) Restraint stress intensifies interstitial K^+ accumulation during severe hypoxia. Front. Pharmacol. **3**:53. doi: 10.3389/fphar.2012.00053*

This article was submitted to Frontiers in Neuropharmacology, a specialty of Frontiers in Pharmacology.